



OPEN

The SensorOverlord predicts the accuracy of measurements with ratiometric biosensors

Julian A. Stanley, Sean B. Johnsen & Javier Apfeld✉

Two-state ratiometric biosensors change conformation and spectral properties in response to specific biochemical inputs. Much effort over the past two decades has been devoted to engineering biosensors specific for ions, nucleotides, amino acids, and biochemical potentials. The utility of these biosensors is diminished by empirical errors in fluorescence-ratio signal measurement, which reduce the range of input values biosensors can measure accurately. Here, we present a formal framework and a web-based tool, the SensorOverlord, that predicts the input range of two-state ratiometric biosensors given the experimental error in measuring their signal. We demonstrate the utility of this tool by predicting the range of values that can be measured accurately by biosensors that detect pH, NAD⁺, NADH, NADPH, histidine, and glutathione redox potential. The SensorOverlord enables users to compare the predicted accuracy of biochemical measurements made with different biosensors, and subsequently select biosensors that are best suited for their experimental needs.

Genetically encoded two-state ratiometric biosensors have revolutionized our ability to monitor a wide variety of biochemical species^{1–8}. The development of these biosensors has enabled the visualization in real-time of the biochemical properties of live animals using fluorescence-ratio microscopy. However, the potential of these biosensors has not been fully realized because the empirical imprecision of their fluorescence-ratio signal measurements reduces the range of biochemical input values those biosensors can measure accurately.

The capacity to make accurate measurements with sensors is important because it enables observers to make confident predictions about the state of a system. Using a thermometer that makes inaccurate temperature measurements can lead to incorrect predictions about the state of a physical system; for example, in predicting whether water will be a solid, a liquid, or a gas. Similarly, using a genetically encoded biosensor that makes inaccurate measurements can lead to incorrect predictions about the state of a biological system.

One application of genetically encoded biosensors is the prediction of proteome reduction–oxidation (redox) states. The human and *C. elegans* proteomes contain ~ 210,000 cysteine residues^{9,10} and ~ 15% of these cysteines are reversibly oxidized¹¹. These protein networks can be understood as markets where cysteines in proteins buy (reduction) and sell (oxidation) pairs of electrons only via a central broker, the abundant glutathione tripeptide¹², resulting in a single price for trading electrons that determines the oxidation of all cysteines in the network (Fig. 1a). In chemical terms, this price is the glutathione redox potential (E_{GSH}): the Nernst potential that quantifies the balance between reduced and oxidized glutathione species. Measuring E_{GSH} accurately is critical because cysteine oxidation modulates the function of hundreds of cytosolic proteins^{13–19} which regulate a wide variety of cellular processes^{19,20}. The mechanisms that regulate E_{GSH} in vivo remained largely unexplored until the development of the E_{GSH} -specific, reduction–oxidation-sensitive Green Fluorescent Protein (roGFP) family of genetically-encoded biosensors^{21–23}. These GFP-derived biosensors include two cysteines that form a (reversible) intramolecular disulfide bond upon oxidation, resulting in spectral changes that can be quantified via fluorescence-ratio microscopy (Fig. 1b)⁸.

We previously used the R12 variant of the roGFP1 biosensor (roGFP1-R12) to measure E_{GSH} in live *C. elegans*¹². In this work, we deployed a mathematical framework that enabled us to map the fluorescence-ratio signal of roGFP1-R12 into glutathione redox potential (E_{GSH}) values using prior information about our microscope's properties and the biosensor's spectral and biochemical properties^{12,22}. Here, we extend that framework to determine how the precision of our fluorescence-ratio signal measurements with the roGFP1-R12 biosensor constrains the range of E_{GSH} values that can be measured accurately. We then generalize this extended framework for all two-state ratiometric biosensors with known spectral and biochemical properties. We demonstrate the

Biology Department, Northeastern University, Boston, MA 02115, USA. ✉email: j.apfeld@northeastern.edu

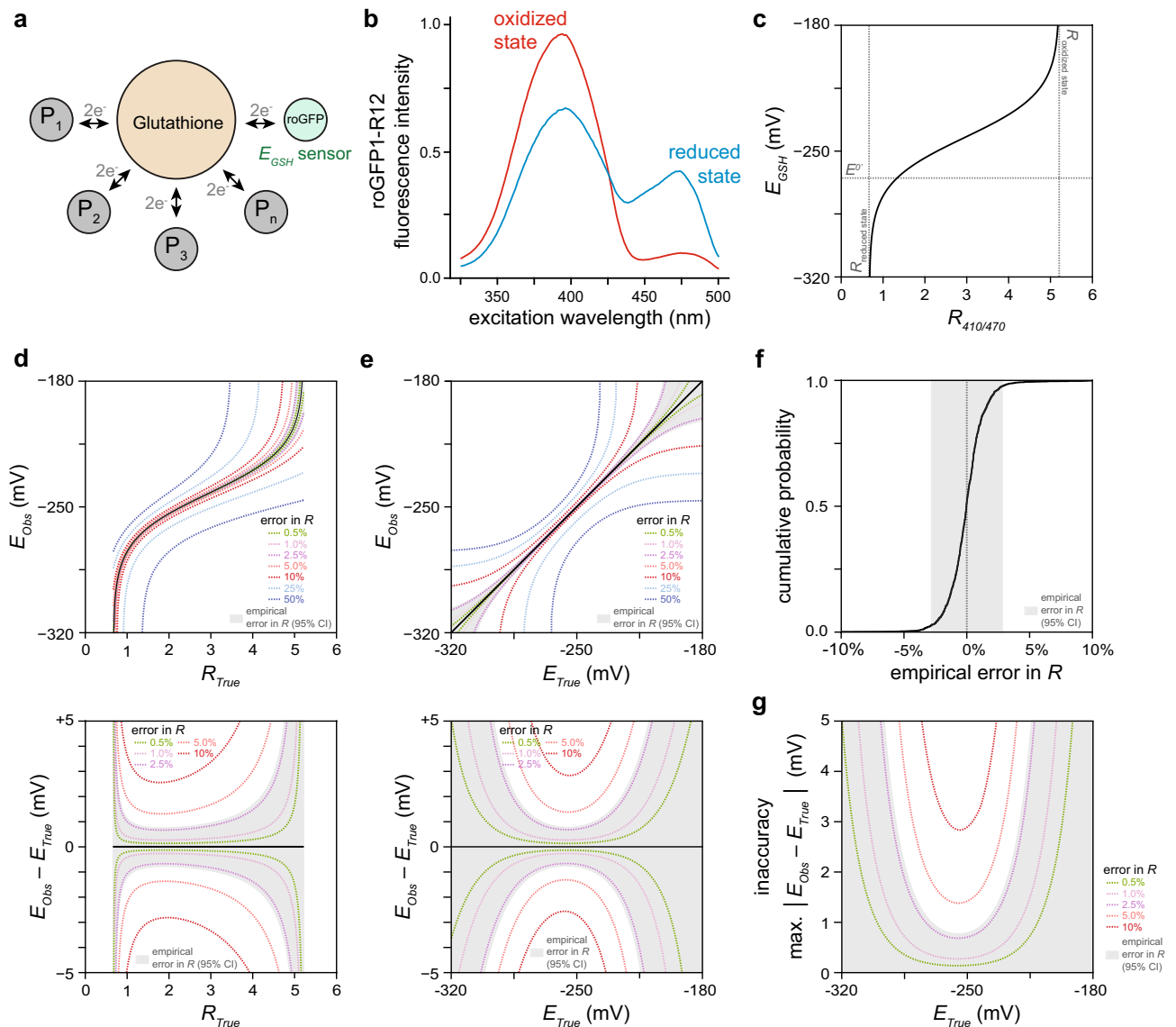


Figure 1. Determining the range of glutathione redox potential E_{GSH} values we can measure accurately with the roGFP1-R12 biosensor. **(a)** Glutathione redox potential (E_{GSH}) directs the oxidation of cysteines in hundreds of proteins in the same direction, resulting in their concerted regulation. **(b)** The reduced and oxidized states of the roGFP1-R12 biosensor have different fluorescence spectra⁸, enabling E_{GSH} measurement via R (fluorescence ratio) microscopy. **(c)** The conversion map from R to E_{GSH} is highly nonlinear. $R_{reduced\ state}$ and $R_{oxidized\ state}$ refer to the ratiometric emission of ensembles of reduced and oxidized biosensors, respectively. E^0 is the standard midpoint potential of the biosensor. **(d)** The top panel shows how measurement errors in R cause observed E_{GSH} values (E_{Obs}) to differ from the true E_{GSH} values (E_{True}) that would be observed if R was measured with no error (R_{True}). The bottom panel shows how the size of an E_{GSH} error ($E_{Obs} - E_{True}$) depends not only on the size of the error in R but also on the value of R . Each dotted curve corresponds to a different fold-change error in R . The shaded region corresponds to the interval encompassing 95% of the predicted E_{Obs} values for each R_{True} value, given our empirical error in R . **(e)** Transforming the map from R_{True} to E_{True} in the top and bottom panels shown in **(d)** produces plots showing how errors in R influence the map from E_{True} to E_{Obs} (top panel) and how the size of an E_{GSH} error depends not only on the size of the error in R but also on the value of E_{True} (bottom panel). Each dotted curve corresponds to a different fold-change error in R . The shaded region shows the interval encompassing 95% of the predicted E_{Obs} values for each E_{True} value, given our empirical error in R . **(f)** Cumulative distribution of the empirical fold error in R in live *C. elegans* expressing the roGFP1-R12 biosensor in the cytosol of the anterior (pm3) muscles of the pharynx, the feeding organ. This error distribution was obtained by aggregating with equal weight the empirical fold error in R of five separate experiments (see Supplementary Note 3). 95% of the errors in R fall within the interval $(-2.8\%, +2.8\%)$, shown shaded in gray. This interval quantifies the precision of our fluorescence-ratio measurements. **(g)** E_{GSH} measurement inaccuracy (the maximum absolute difference between E_{True} and E_{Obs}) decreases with increased precision of R measurement. Each dotted curve corresponds to a different precision of R measurement. The shaded region shows the interval encompassing 95% of the predicted E_{GSH} measurement inaccuracies for each E_{True} value, given our empirical error in R .

utility of this new framework by: (1) determining the range of E_{GSH} values that we can measure accurately in live *C. elegans* with the roGFP1-R12 biosensor; (2) quantifying how much that range of E_{GSH} values is expanded by increasing the precision of our imaging and image-analysis methods; (3) identifying which biosensors are best suited for accurately measuring different ranges of E_{GSH} , pH, and the concentrations of nucleotides and amino acids; (4) identifying underused biosensors; and (5) identifying where new biosensors are needed.

To help the community identify biosensors that are well-suited for their experimental needs, we developed a web-based tool, the SensorOverlord (<https://www.sensoroverlord.org>), that implements all of these analyses with a user-friendly interface.

Results

Predicting the accuracy of a glutathione redox potential biosensor. In our previous work, we used roGFP1-R12 to measure E_{GSH} in live *C. elegans*¹². To map R (fluorescence ratio) measurements into E_{GSH} values, we determined three conversion factors that quantify the properties of our imaging microscope and the spectral differences between the reduced and oxidized states of the biosensor (Supplementary Note S1). Measuring E_{GSH} instead of R enabled us to make predictions about how the oxidation state of the network of cysteines trading electrons with glutathione is influenced by genetic determinants and environmental factors¹². However, those predictions require that E_{GSH} be measured accurately. Therefore, we set out to determine how the precision of our fluorescence-ratio microscopy influenced the range of E_{GSH} values we could measure accurately.

We first modeled how errors in fluorescence-ratio measurement influenced E_{GSH} errors. The conversion map from R to E_{GSH} is highly nonlinear (Fig. 1c). As a result, the size of an E_{GSH} error depends not only on the size of the error in R but also on the value of R (Fig. 1d): as R approaches its lower and upper bounds E_{GSH} errors increase rapidly (Supplementary Note S2). Thus, even a small difference between observed and true R values (R_{Obs} and R_{True} , respectively) can lead to a large difference between observed and true E_{GSH} values (E_{Obs} and E_{True} , respectively) (Fig. 1d).

We then determined the size of our fluorescence-ratio measurement errors. We quantified the precision of our fluorescence-ratio measurements in live *C. elegans* expressing the roGFP1-R12 biosensor in the cytosol of the muscles of the pharynx, the feeding organ. This retrospective analysis of 10,572 images showed that our errors in R were proportional to R —that is, $R_{Obs} = R_{True} * (1 + error)$ (Supplementary Note S3). Within a given experiment, the size of the relative error in R was invariant over the range of all possible R values (Supplementary Note S3). The size of the relative error in R , however, varied up to three-fold between experiments (Supplementary Note S3). Differences in the proportion of animals moving during imaging accounted for most of the variation in the relative error in R across experiments (S.B.J., J.A.S., and J.A., manuscript in preparation). Our analysis indicated that, in a typical experiment, the median relative error in R was zero and 95% of the relative errors in R were in the interval $(-2.8\%, +2.8\%)$ (Fig. 1f). These 95% confidence bounds quantified the precision of our fluorescence-ratio measurements.

Last, we determined how the empirical precision of our fluorescence-ratio measurements influenced the accuracy of individual E_{GSH} observations. Knowing the precision of our R measurements enabled us to determine the 95% confidence bounds of E_{Obs} as a function of R_{True} (Fig. 1d). Converting R_{True} into E_{True} produced a map of how the 95% confidence bounds of E_{Obs} varied as a function of E_{True} (Fig. 1e). The maximum absolute difference between E_{True} and either the upper or lower 95% confidence bound of E_{Obs} represents the inaccuracy of our E_{GSH} measurements (Fig. 1g). Our mathematical modeling indicated that the precision of R measurements, the biochemical and biophysical properties of the biosensor, and the choice of excitation wavelengths used in our experiments all influenced the E_{GSH} values that we could measure most accurately (Supplementary Note S4). E_{GSH} inaccuracy rapidly increased as E_{True} moved farther away from those values.

This analysis enabled us to extract the range of E_{GSH} values that our biosensor was well-suited to measure at a given level of E_{GSH} inaccuracy (Fig. 1g). For example, the range of E_{Obs} values we could measure with an inaccuracy of 2 mV was between -284 and -234 mV. This range encompassed all E_{GSH} values we observed in wild-type nematodes under normal conditions $(-278$ to -262 mV) and under oxidative stress $(-278$ to -250 mV)¹², indicating that our experimental set up was well-suited to measure the E_{GSH} values that *C. elegans* feeding muscles exhibited in vivo: 95% of the individual E_{GSH} observations deviated from their true value by less than 2 mV.

Balancing the need for accurate measurements with the constraints of microscopy. Our analytical framework provides a criterion for determining if it is possible to measure E_{GSH} accurately. Scientific needs demand accurate observations, but experimental approaches constrain the extent to which observations can be made accurately. The trade-off between these scientific and experimental constraints can be visualized in a phase diagram (Fig. 2). The precision of R measurements determines the range of E_{GSH} values that is possible to measure at a specific inaccuracy level (Fig. 2). For values outside that range, it is impossible to guarantee that an observation will be accurate. Scientific needs impose a maximum tolerable inaccuracy beyond which observations are too inaccurate and, therefore, not useful. Together, these constraints determine whether it is possible to measure E_{GSH} accurately (Fig. 2).

Retrospectively increasing measurement accuracy with improved image analysis. To increase the range of E_{GSH} values that we could measure accurately, we set out to improve our image-analysis methods. Movement of live *C. elegans* during image acquisition lowers the precision of fluorescence-ratio measurements

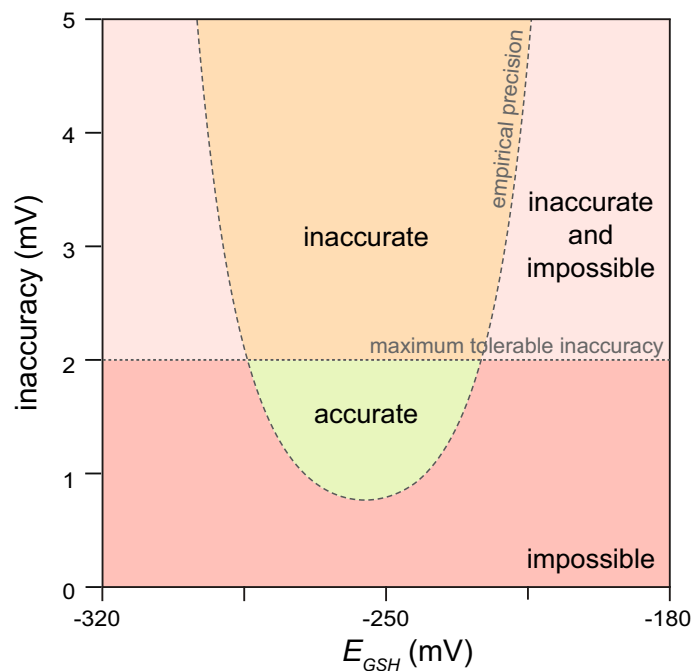


Figure 2. Balancing the need for accurate measurements with the constraints of microscopy. The empirical precision of our R measurements determines the range of E_{GSH} values that is possible to measure at a specific inaccuracy level. Values outside that range are impossible to measure accurately (red and light red regions). Scientific needs impose a maximum tolerable inaccuracy beyond which observations are too inaccurate and, therefore, not useful (light red and orange regions). Together, these constraints determine whether it is possible to accurately measure E_{GSH} (green region).

in individual pharyngeal muscles. In a typical experiment 21% of animals moved during imaging. We developed a new image-feature registration algorithm that corrects for displacement and deformation of the muscles along the anterior–posterior axis of the pharynx (S.B.J., J.A.S., and J.A., manuscript in preparation). This new image-analysis algorithm reduced the relative error in R along most positions in the pharynx, especially in the boundaries between adjacent muscles and in the muscles of the anterior and posterior bulbs. For example, in the pm7 muscles of the posterior bulb, the new algorithm reduced the interval with 95% of the relative errors in R from ± 4.3 to $\pm 2.6\%$ in moving animals and from ± 2.0 to $\pm 1.9\%$ in stationary animals. As a result, the new algorithm increased the accuracy with which we could measure E_{GSH} and thereby expanded the range of E_{GSH} values that we could measure accurately in past experiments (Fig. 3a).

Comparing glutathione redox potential biosensors. We determined the ranges of E_{GSH} values that we could have measured accurately had we used different biosensors. Theoretical modeling indicated that the accuracy of a biosensor is influenced by the choice of wavelengths used for biosensor excitation, and by the biosensor's dynamic range and midpoint-potential (E^0 , the price point where a biosensor is 50% likely to sell its electrons) (Supplementary Note S4). These biosensor physical and chemical properties vary among all existing roGFP-based biosensors (Supplementary Note S5). We estimated the conversion factors that map fluorescence-ratio measurements into E_{GSH} values for the eleven roGFP-based biosensors with published midpoint potentials and fluorescence spectra (Supplementary Note S5). This enabled us to determine the E_{GSH} inaccuracy we would expect to observe had we measured E_{GSH} in the feeding muscles of live *C. elegans* with each of those biosensors instead of roGFP1-R12 (Fig. 3b and Supplementary Note S5). This analysis enabled us to identify which biosensors would measure E_{GSH} most accurately under our experimental conditions: roGFP5 for E_{GSH} values below -297 mV, roGFP2 for E_{GSH} values from -296 to -258 mV, roGFP1-R12 for E_{GSH} values from -257 to -240 mV, and roGFP1-iE for E_{GSH} values above -239 mV. We note that often many biosensors were predicted to have comparable accuracies (Fig. 3b).

This analysis helped us identify underused biosensors. Neither roGFP3 nor roGFP5 has ever been used *in vivo*, yet we predict that these biosensors would be the most accurate biosensors for low E_{GSH} values such as those expected for the mitochondrial matrix. We currently disfavor roGFP5, even though this biosensor was predicted to be more accurate than roGFP3, because roGFP5 can potentially form more than one type of internal disulfide bridge due to its two additional cysteines; a better understanding of roGFP5's biochemistry is warranted given its potential utility.

Comparison of the predicted accuracy of biosensors originally designed for similar purposes enabled us to identify the variables that explain why one biosensor was predicted to be more accurate than another (Supplementary Note S6). For example, both roGFP1-iE and roGFP2-iL were designed to have higher midpoint potentials than previous roGFPs, making them more suitable for measuring the higher E_{GSH} values common in the endoplasmic reticulum^{24,25}. However, while roGFP1-iE has a higher midpoint potential than roGFP2-iL, it is predicted to be more inaccurate than roGFP2-iL even for measuring higher E_{GSH} values. The higher dynamic range of roGFP2-iL makes it a more accurate E_{GSH} biosensor than roGFP1-iE.

Identifying where new glutathione redox potential biosensors are needed. We predicted the E_{GSH} inaccuracy that we would observe if we measured E_{GSH} in the feeding muscles of live *C. elegans* with the most accurate biosensor for each E_{GSH} value. Using a phase diagram, we visualized the trade-off between our scientific need for accuracy and the experimental constraints imposed by the precision of our R measurements and the properties of existing biosensors (Fig. 3c). This analysis indicated that we lack biosensors well-suited to measure E_{GSH} values above -177 mV or below -337 mV with at least 10 mV accuracy.

A general framework to predict the accuracy of two-state ratiometric biosensors. To establish a general criterion for determining whether a two-state biosensor is well-suited to measure its input accurately, we generalized the analysis framework for glutathione redox potential biosensors to all ratiometric two-state single-ligand-binding biosensors (Supplementary Notes S1, S5, S7). To demonstrate the utility of the generalized framework, we applied it to biosensors that measure pH and small molecules, including histidine, NAD⁺, NADH, and NADPH. For each biosensor with a known affinity constant and fluorescence spectra, we derived the conversion factors that map its fluorescence-ratio to pH or ligand concentration (Supplementary Notes S8, S9). We then determined the pH and ligand concentration ranges that each biosensor would be well-suited to measure accurately given the precision of our R measurements and after selecting optimal excitation or emission filters for each biosensor (Fig. 4a,b and Supplementary Notes S8, S9).

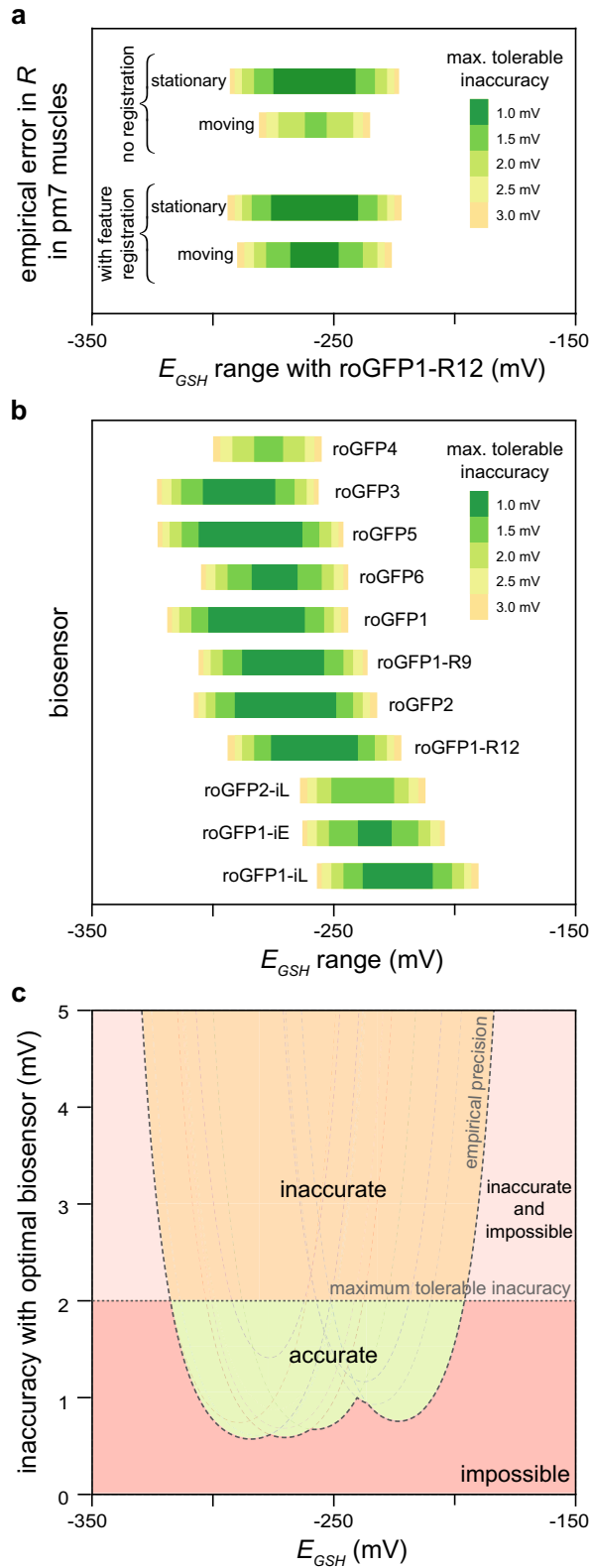
Our comparison of the predicted accuracy of nine ratiometric pH biosensors identified optimal biosensors for pH measurement with dual-excitation red-fluorescent pH biosensors, dual-excitation green-fluorescent pH biosensors, and single-excitation dual-emission pH biosensors (Fig. 4a). The NADH-specific Frex biosensor⁶ had a higher predicted accuracy than the FrexH biosensor⁶, as a result of its higher dynamic range (Fig. 4b). The NADPH-specific iNAP1 biosensor⁷ was predicted to more accurately measure NADPH concentration than the iNAP1-mCherry biosensor (Fig. 4b). The iNAP1-mCherry biosensor sacrifices the iNAP1 dynamic range in one excitation band with pH-sensitive fluorescence, enabling pH-resistant NADPH measurement but lowering this biosensor's accuracy.

A web-based tool that predicts biosensor accuracy. To help the community find biosensors that are well-suited for their experimental needs, we developed the SensorOverlord toolkit. This open-source S4 class-based R package implements all the analyses described here. We also built a user-friendly web application, available at <https://www.sensoroverlord.org> (Fig. 5). The SensorOverlord toolkit enables users to model how the precision of their fluorescence-ratio signal measurements and their microscopy configuration constrain the range of input values that their biosensor is well-suited to measure accurately (Supplementary Note S10).

The SensorOverlord R package provides a set of classes, methods, and functions with which users can analyze their microscopy accuracy. Briefly, users can create a *Sensor* object by (1) programmatically uploading an excitation-emission spectrum, (2) inputting biophysical parameters of the biosensor, or (3) querying a biosensor database containing the excitation-emission spectra of the biosensors discussed in this manuscript. *Sensor* objects can then be used to generate maps between R and the predicted inaccuracy of E_{GSH} , pH, and p[Ligand] at different levels of empirically-determined error in the measurement of R . The package also enables users to directly create *Spectra* excitation-emission plots, and to plot the predicted inaccuracy and predicted suitable range of any custom E_{GSH} , pH, or ligand-sensitive two-state biosensor. We designed the package so users can not only recreate the analysis presented here, but also quickly and easily apply the SensorOverlord framework to other biosensors and experimental configurations.

The SensorOverlord web application makes the SensorOverlord R package accessible via a non-programmatic graphical user interface that can be accessed through any modern web browser. Users can generate a *Sensor* object by (1) selecting a biosensor from a biosensor database via a dropdown menu, (2) inputting empirically-obtained biophysical parameters into text boxes, or (3) interactively uploading a .csv file with excitation-emission spectrum values. The application then prompts users to provide an empirical error in the measurement of R , the accuracies at which they wish to make measurements, and the excitation or emission wavelength intervals used for ratiometric imaging. Once a user inputs these parameters, they click a button to generate two figures: (1) a static plot of the suitable ranges of the current biosensor, and (2) an interactive plot of the current biosensor's measurement accuracy as a function of the biochemical parameter being measured (Fig. 5). Besides increasing the accessibility of the analysis presented here, the SensorOverlord web application enables users to more quickly and easily experiment with how modifying model parameters affects the predicted accuracy of measurements with different biosensors.

Documentation for the SensorOverlord toolkit, alongside updated links to the source code and web application, can be found at <https://apfeldlab.github.io/SensorOverlord/>.



◀ **Figure 3.** Predicted accuracy of glutathione redox potential biosensors. **(a)** Predicted accuracy gains from improved image analysis in the pm7 (posterior) feeding muscles of live *C. elegans* expressing the roGFP1-R12 biosensor. Animals that moved during image acquisition showed a higher R measurement error than stationary animals. A feature-registration algorithm increased the precision of R measurements, retrospectively expanding the range of E_{GSH} values that we could measure accurately. The colored bars denote the range of E_{GSH} values where we have 95% confidence that an individual E_{GSH} observation would deviate from its true value by less than the error denoted by the color of the bar. **(b)** Predictions of the ranges of E_{GSH} values that we expect to measure accurately in pm3 pharyngeal muscles with eleven roGFP-based biosensors given the empirical precision of our R measurements. Coloring of bars as in **(a)**. **(c)** The empirical precision of our R measurements determines the range of E_{GSH} values that would be possible to measure at a specific inaccuracy level if we measured E_{GSH} in the pharyngeal muscles of live *C. elegans* with the most accurate roGFP biosensor for each E_{GSH} value. Values outside that range are impossible to measure accurately (red and light red regions). Scientific needs impose a maximum tolerable inaccuracy beyond which observations are too inaccurate and, therefore, not useful (light red and orange regions). Together, these constraints determine whether it is possible to accurately measure E_{GSH} with the eleven roGFP biosensors (green region). The dotted curves correspond to the predicted E_{GSH} inaccuracies of each of the eleven roGFP biosensors shown in **(b)**, given the precision of our R measurements.

Discussion

The SensorOverlord toolkit enables users to predict the accuracy of concentrations and chemical potentials derived from fluorescence ratio measurements with two-state biosensors. This tool enables users to select biosensors predicted to be most accurate for measuring specific ranges of biochemical values. The SensorOverlord also enables users to quantify the extent to which increasing the precision of their fluorescence-ratio measurements would increase the predicted accuracy of their biochemical measurements with an individual biosensor. Therefore, this tool can be used to quantify the accuracy gains resulting from improving experimental practices, and from refining image acquisition, registration, and analysis methods.

A wide variety of factors can influence the precision of fluorescence-ratio measurement. In our experience, the degree of immobilization of live specimens during image acquisition can influence the precision of fluorescence-ratio measurements by a factor of three, leading to large differences in the predicted accuracy of biochemical measurements. The SensorOverlord enables researchers to disclose the predicted accuracy of the concentrations and chemical potentials that they measure, simply by reporting the precision of their fluorescence-ratio measurements—similar to how manufacturers use tolerance ratings to disclose how often the quality of their products is expected to deviate from a standard. The broader scientific community may, in turn, adopt appropriate maximum tolerable inaccuracy standards for specific biochemical measurements.

Prediction of the input values of two-state ratiometric biosensors from their ratiometric fluorescence requires knowledge of conversion factors that quantify the biosensor's biochemical and biophysical properties. The values of these factors could be influenced by the cellular environment where the biosensor is expressed. Our studies with roGFP1-R12 in the cytosol of *C. elegans* feeding muscles showed that the biosensor's *in vivo* dynamic range was 7.8, slightly higher than the 5.0 dynamic range of the purified biosensor *in vitro*; as a result, the biosensor had a higher predicted accuracy than expected from its properties *in vitro* (Supplementary Note S5.2). This example highlights the need to determine those conversion factors under the relevant experimental conditions, which often is very challenging. A better understanding of how the spectral and biochemical properties of each biosensor are influenced by the temperature, pH, ionic strength, and osmotic strength of the environment surrounding the biosensor would enable better prediction of the properties of the biosensor *in vivo*.

We hope that the SensorOverlord motivates the development of new biosensors, microscopy techniques, and image-analysis methods, by enabling biosensor developers and users to quantify the accuracy gains that would result from modifying the biochemical and spectral properties of their biosensors and from increasing the precision of their fluorescence-ratio measurements.

Methods

Code availability. Mathematical modeling was performed in the R language and environment for statistical computing (v3.6.0)²⁶. The web application and associated visualizations were developed with the R packages ggplot2 (v3.1.1)²⁷, Shiny (v1.3.2)²⁸, and plotly (v4.9.2)²⁹. Source code for the SensorOverlord is available at <https://apfeldlab.github.io/SensorOverlord/>.

Statistical analysis. All statistical analyses were performed in JMP (SAS). We tested for differences in the average R among groups using ANOVA. We used the Tukey HSD post-hoc test to determine which pairs of groups in the sample differ, in cases where more than two groups were compared. We used least-squares regression to quantify the dependency on R of the absolute error in R and the absolute relative error in R .

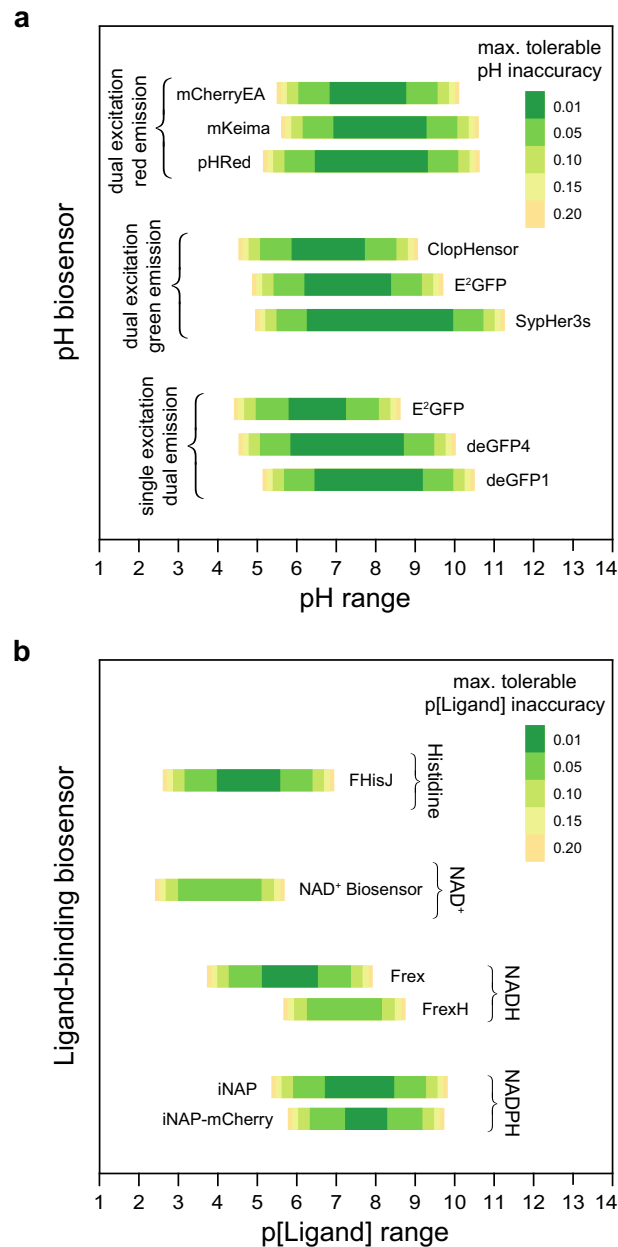


Figure 4. Predicted accuracy of pH and ligand-binding biosensors. Predictions of the ranges of pH (a), and histidine, NAD⁺, NADH, and NADPH values (b) that we expect to measure accurately in pm3 pharyngeal muscles with existing biosensors given the empirical precision of our *R* measurements and selecting optimal excitation or emission filters for each biosensor. The E²GFP biosensor can be used in two different modalities, dual-excitation green-fluorescence and single-excitation dual-emission. Differences in the predicted pH inaccuracy of this biosensor under each imaging modality arise from the differences between the values in each imaging modality of this biosensor's overall dynamic range and dynamic range in the second wavelength (Supplementary Note 8). The colored bars denote the range of values of the biosensor's biochemical input where we have 95% confidence that an individual observation would deviate from its true value by less than the error denoted by the color of the bar. p[Ligand] is the negative base 10 logarithm of the Molar concentration of the biosensor's ligand.

S.O. Home Main Analysis More Information

Sensor Parameters

What sensor would you like to use?

Select a sensor
roGFP1

We have loaded a few pre-analysed sensors to get you started. Feel free to choose one of those from the dropdown box.

Once you're comfortable, select 'Custom', and then scroll to the bottom of the page to input the characteristics of your sensor of choice.

What is your microscopy precision, and how accurate would you like to be?

Relative Microscopy Imprecision: 0.01
Accuracy (comma-separated): 0.5,1.0,1.5

You'll need to determine your microscopy imprecision empirically. For reference, 95% of our observed ratios deviate from their true value by no more than 2.8%, but that can vary from 1% to 4% depending on image analysis methods and experimental conditions.

Accuracy can be determined as you see fit!

What wavelengths are you using to make your measurements?

First Wavelength: 410
Second Wavelength: 470
Band Size (1st Wavelength): 10
Band Size (2nd Wavelength): 10

You may find that adjusting your wavelengths or narrowing your band size may affect the ultimate accuracy of your measurements.

Run/Update Analysis

Suitable Range

Predicted Inaccuracy Plot

Custom Sensor Input

SensorOverlord needs Rmin, Rmax, delta, and midpoint values. It can either determine some of those from an uploaded spectra file ('Upload Spectra' tab), or you can provide those parameters ('Input Characteristics' tab).

Upload Spectra Input Characteristics

Upload spectra as .csv
Browse... No file selected

Sensor Name
My Sensor

Sensor Type
 Redox
 pH
 Other

Midpoint Value (E0, pKa, etc) Note: Ignored for 'other' sensor type
1

Use This Sensor

Sensor	roGFP1
Rreduced	3.68
Roxidized	24.61
Dynamic Range	6.69

Figure 5. SensorOverlord web application. The SensorOverlord toolkit enables users to model how the range of input values that their biosensor is well-suited to measure accurately is constrained by the user's fluorescence-ratio signal measurement precision and microscopy configuration.

Data availability

The datasets used and/or analyzed during the current study are available from the corresponding author on reasonable request.

Received: 22 May 2020; Accepted: 24 September 2020

Published online: 08 October 2020

References

- Hanson, G. T. *et al.* Investigating mitochondrial redox potential with redox-sensitive green fluorescent protein indicators. *J. Biol. Chem.* **279**, 13044–13053 (2004).
- Tantama, M., Hung, Y. P. & Yellen, G. Imaging intracellular pH in live cells with a genetically encoded red fluorescent protein sensor. *J. Am. Chem. Soc.* **133**, 10034–10037. <https://doi.org/10.1021/ja202902d> (2011).
- Poburko, D., Santo-Domingo, J. & Demaurex, N. Dynamic regulation of the mitochondrial proton gradient during cytosolic calcium elevations. *J. Biol. Chem.* **286**, 11672–11684. <https://doi.org/10.1074/jbc.M110.159962> (2011).
- Hu, H. *et al.* A genetically encoded toolkit for tracking live-cell histidine dynamics in space and time. *Sci. Rep.* **7**, 43479. <https://doi.org/10.1038/srep43479> (2017).
- Cambronne, X. A. *et al.* Biosensor reveals multiple sources for mitochondrial NAD(+). *Science* **352**, 1474–1477. <https://doi.org/10.1126/science.aad5168> (2016).
- Zhao, Y. *et al.* Genetically encoded fluorescent sensors for intracellular NADH detection. *Cell Metab.* **14**, 555–566. <https://doi.org/10.1016/j.cmet.2011.09.004> (2011).
- Tao, R. *et al.* Genetically encoded fluorescent sensors reveal dynamic regulation of NADPH metabolism. *Nat. Methods* **14**, 720–728. <https://doi.org/10.1038/nmeth.4306> (2017).
- Cannon, M. B. & Remington, S. J. Re-engineering redox-sensitive green fluorescent protein for improved response rate. *Protein Sci.* **15**, 45–57 (2006).
- Jones, D. P. Radical-free biology of oxidative stress. *Am. J. Physiol. Cell Physiol.* **295**, C849–868. <https://doi.org/10.1152/ajpcell.00283.2008> (2008).
- Moosmann, B. & Behl, C. Mitochondrially encoded cysteine predicts animal lifespan. *Aging Cell* **7**, 32–46. <https://doi.org/10.1111/j.1474-9726.2007.00349.x> (2008).
- Hansen, R. E., Roth, D. & Winther, J. R. Quantifying the global cellular thiol-disulfide status. *Proc. Natl. Acad. Sci. USA* **106**, 422–427. <https://doi.org/10.1073/pnas.0812149106> (2009).
- Romero-Aristizabal, C., Marks, D. S., Fontana, W. & Apfeld, J. Regulated spatial organization and sensitivity of cytosolic protein oxidation in *Caenorhabditis elegans*. *Nat. Commun.* **5**, 5020. <https://doi.org/10.1038/ncomms6020> (2014).
- Gilbert, H. F. Biological disulfides: the third messenger? Modulation of phosphofruktokinase activity by thiol/disulfide exchange. *J. Biol. Chem.* **257**, 12086–12091 (1982).
- Gilbert, H. F. Molecular and cellular aspects of thiol-disulfide exchange. *Adv. Enzymol. Relat. Areas Mol. Biol.* **63**, 69–172 (1990).
- Corcoran, A. & Cotter, T. G. Redox regulation of protein kinases. *FEBS J.* **280**, 1944–1965. <https://doi.org/10.1111/febs.12224> (2013).
- Fuller, W. *et al.* Regulation of the cardiac sodium pump. *Cell Mol. Life Sci.* **70**, 1357–1380. <https://doi.org/10.1007/s00018-012-1134-y> (2013).
- Yang, Y., Jin, X. & Jiang, C. S-glutathionylation of ion channels: insights into the regulation of channel functions, thiol modification crosstalk and mechanosensing. *Antioxid Redox Signal* **6**, 937–951. <https://doi.org/10.1089/ars.2013.5483> (2013).
- de Keizer, P. L., Burgering, B. M. & Dansen, T. B. Forkhead box o as a sensor, mediator, and regulator of redox signaling. *Antioxid Redox Signal* **14**, 1093–1106. <https://doi.org/10.1089/ars.2010.3403> (2011).
- Pastore, A. & Piemonte, F. S-Glutathionylation signaling in cell biology: progress and prospects. *Eur. J. Pharm. Sci.* **46**, 279–292. <https://doi.org/10.1016/j.ejps.2012.03.010> (2012).
- Sakai, J. *et al.* Reactive oxygen species-induced actin glutathionylation controls actin dynamics in neutrophils. *Immunity* **37**, 1037–1049. <https://doi.org/10.1016/j.immuni.2012.08.017> (2012).
- Meyer, A. J. *et al.* Redox-sensitive GFP in *Arabidopsis thaliana* is a quantitative biosensor for the redox potential of the cellular glutathione redox buffer. *Plant J. Cell Mol. Biol.* **52**, 973–986. <https://doi.org/10.1111/j.1365-313X.2007.03280.x> (2007).
- Meyer, A. J. & Dick, T. P. Fluorescent protein-based redox probes. *Antioxid. Redox. Signal* **13**, 621–650 (2010).
- Schwarzlander, M. *et al.* Confocal imaging of glutathione redox potential in living plant cells. *J. Microsc.* **231**, 299–316. <https://doi.org/10.1111/j.1365-2818.2008.02030.x> (2008).
- Lohman, J. R. & Remington, S. J. Development of a family of redox-sensitive green fluorescent protein indicators for use in relatively oxidizing subcellular environments. *Biochemistry* **47**, 8678–8688. <https://doi.org/10.1021/bi800498g> (2008).
- Aller, I., Rouhier, N. & Meyer, A. J. Development of roGFP2-derived redox probes for measurement of the glutathione redox potential in the cytosol of severely glutathione-deficient *rml1* seedlings. *Front. Plant Sci* **4**, 506. <https://doi.org/10.3389/fpls.2013.00506> (2013).
- R Development Core Team. *R: A language and environment for statistical computing*. <https://www.R-project.org/> (R Foundation for Statistical Computing, Vienna, 2019).
- Wickham, H. *Ggplot2: elegant graphics for data analysis* (Springer, 2009).
- Chang, W., Cheng, J., Allaire, J., Xie, Y. & McPherson, J. *Shiny: Web Application Framework for R*. R package version 1.0.3. <https://shiny.rstudio.com/> (2017).
- Sievert, C. *Interactive web-based data visualization with R, plotly, and shiny* (CRC Press, Taylor and Francis Group, 2020).

Acknowledgements

We thank Jeff Bouffard, Jennifer Whangbo, Marianne Konikoff, Jodie Schiffer, Frank Servello, and Yuyan Xu for critical reading and detailed comments on our manuscript. We benefitted from discussions with members of Javier Apfeld's and Erin Cram's labs. Some strains were provided by the CGC, which is funded by NIH Office of Research Infrastructure Programs (P40 OD010440). The research was supported by a Northeastern TIER1 award and a National Science Foundation CAREER grant (1750065) to J.A.

Author contributions

J.A.S. and J.A. conceived and designed the analysis framework. J.A.S. designed and implemented the SensorOverlord software. S.B.J. analyzed fluorescence-ratio measurement precision. J.A.S. and J.A. analyzed data, interpreted results and wrote the manuscript.

Competing interests

The authors declare no competing interests.

Additional information

Supplementary information is available for this paper at <https://doi.org/10.1038/s41598-020-73987-0>.

Correspondence and requests for materials should be addressed to J.A.

Reprints and permissions information is available at www.nature.com/reprints.

Publisher's note Springer Nature remains neutral with regard to jurisdictional claims in published maps and institutional affiliations.



Open Access This article is licensed under a Creative Commons Attribution 4.0 International License, which permits use, sharing, adaptation, distribution and reproduction in any medium or format, as long as you give appropriate credit to the original author(s) and the source, provide a link to the Creative Commons licence, and indicate if changes were made. The images or other third party material in this article are included in the article's Creative Commons licence, unless indicated otherwise in a credit line to the material. If material is not included in the article's Creative Commons licence and your intended use is not permitted by statutory regulation or exceeds the permitted use, you will need to obtain permission directly from the copyright holder. To view a copy of this licence, visit <http://creativecommons.org/licenses/by/4.0/>.

© The Author(s) 2020